LA-UR-15-29694 (Accepted Manuscript)

High pressure elasticity and thermal properties of depleted uranium

Jacobsen, Matthew
Velisavljevic, Nenad

To be published in: Journal of Applied Physics

DOI to publisher's version: 10.1063/1.4948300

Permalink to record: http://permalink.lanl.gov/object/view?what=info:lanl-repo/lareport/LA-UR-15-29694

High pressure elasticity and thermal properties of depleted uranium

M.K. Jacobsen[1, a)] and N. Velisavljevic[1, b)]
Shock and Detonation Physics (M-9), Los Alamos National Laboratory, Los Alamos, NM 87544 USA

(Dated: 11 April 2016)

Studies of the phase diagram of uranium have revealed a wealth of high pressure and temperature phases. Under ambient conditions the crystal structure is well defined up to 100 gigapascals (GPa), but very little information on thermal conduction or elasticity is available over this same range. This work has applied ultrasonic interferometry to determine the elasticity, mechanical, and thermal properties of depleted uranium to 4.5 GPa. Results show general strengthening with applied load, including an overall increase in acoustic thermal conductivity. Further implications are discussed within. This work presents the first high pressure studies of the elasticity and thermal properties of depleted uranium metal and the first real-world application of a previously developed containment system for making such measurements.

PACS numbers: 64.30.-t, 63.20.-e, 62.50.-p
Keywords: High Pressure, Elasticity, Uranium

I. INTRODUCTION

Uranium, which occupies an important central position in the early actinides, is well known for its many uses. In particular, depleted uranium and its alloys are important engineering materials due to their high density. It is well known that depleted uranium can be alloyed to effect improvements in many elastic and plastic related deformation properties, to improve corrosion resistance, and to allow flexible heat treatability[1–3].

However, most studies of uranium have focused on the low temperature properties[4–7] or high pressure/high temperature structure[8]. Overall, such information is useful and necessary to better understand the f-shell dynamics, but does not provide all information needed for applications. This can be particularly evident through theoretical studies[9], which explore the elasticity and mechanical properties from a theoretical viewpoint. In contrast, experimental studies[8] use *in situ* diamond anvil cell (DAC) x-ray diffraction and laser heating techniques to explore the phase diagram up to 100 GPa and high temperature. Studies of this sort help to determine the isothermal modulus and phase boundaries, but do not extend to full elasticity or thermal properties. As a result, it is necessary that high pressure techniques move beyond just x-ray diffraction.

One technique in this area is ultrasonic interferometry (UI), which discerns information on sound speeds and elastic/thermal properties, through the application of acoustic impedance generated reflections at interfaces between materials. Well established for the study of mineral species, UI involves generation of a sound wave outside the pressurized region and components of the pressure system are chosen to propagate this sound wave to the sample. By combining such studies with x-ray measurements and radiography, it is possible to directly determine sound velocities for a wide array of sample species and indirectly determine several other parameters. Further details of the technique are given in excellent references[10–13].

In this work, we present the first ultrasonic, high-pressure study of depleted uranium. This is accomplished through the combined use of x-ray diffraction, radiography, and ultrasonic interferometry. Through the application of these techniques, we have been able to determine high pressure elastic and x-ray equations of state, elastic moduli, and a variety of thermal properties.

II. EXPERIMENTAL DETAILS AND DATA ANALYSIS

Depleted uranium samples (LANL, 99.5% purity) were prepared in cylindrical, metallic form, with a diameter of 0.8 mm and thickness of 0.5 mm. These samples were prepared in standard 13 mm ultrasonic cell assemblies (Fig. 1), used with the Paris-Edinburgh Press at beamline 16-BM-B of the Advanced Photon Source. Specific details on the press setup and ultrasonic experiments are described in previous reports[13,14]. Sample assemblies were loaded in an in-house constructed containment assembly[14] to prevent contamination in case of cell assembly failure.

Combined ultrasonic interferometry/x-ray diffraction/x-ray radiography techniques were used to gather data on the sample as the PE press hydraulic load increased up to 5500 psi (corresponding to $\approx$ 4.5 GPa on the sample). Energy dispersive x-ray diffraction spectra have been analyzed using MDI's JADE software[16] with LeBail structural refinement on both the MgO and U sample patterns at each pressure point. An example diffraction pattern and refinement for this are shown in Figure 2. In the refinement, a pseudo-Voight peak shape was assumed and the peak full-width at half-maximum values were refined for each

[a)] mjacobsen@lanl.gov
[b)] nenad@lanl.gov

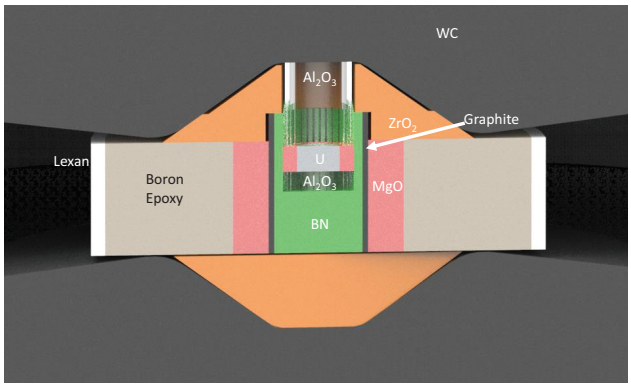

FIG. 1. The sample assembly used is a collection of materials chosen for their strength/deformation properties in addition to the x-ray transparency. The sample is contained in an MgO ring, and faced on the polished end faces with comparatively polished Al_2O_3. The remainder of the parts for this sample assembly are standard for the 13 mm diameter cell assembly (outer diameter of the Lexan Ring). The alumina polished faces serve to produce reflection from interfaces between different materials for the ultrasonic interferometry measurement. The MgO ring is used as a pressure calibrant[15], in addition to confining the sample. (Color online.)

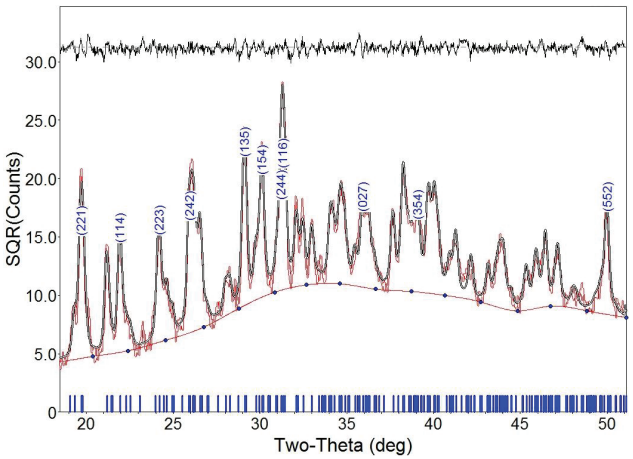

FIG. 2. Energy dispersive x-ray patterns were collected independently for both the sample and the MgO sleeve, using an Ge point detector at 15° in two-theta space. An example pattern for the sample is shown (0.3 GPa, 1183 psi), with refined LeBail structure fit shown. In this figure, the red line is the measured pattern, the double black line is the LeBail fit, and the red dotted line represents the background. The blue dashes at the bottom represent the peak positions and the black line at the top is the difference spectrum. HKL labels for some peaks are shown over the pattern. (Color online.)

peak individually.

Radiographs were used to determine sample lengths. Sample length (L) was determined using contrast difference at the edge of the sample, with an automated searching procedure in Igor Pro[17] being used. Estimates for the sample edges are input and the system searches

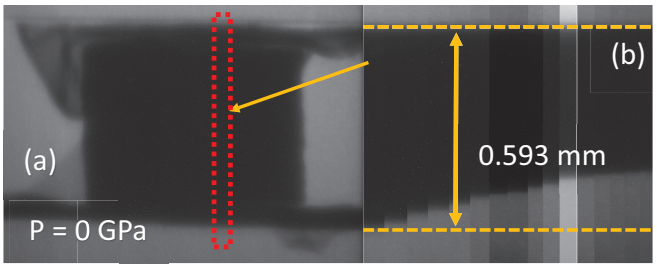

FIG. 3. X-ray radiographs are taken of the sample at each pressure point investigated. Using an automated contrast fitting algorithm, the top and bottom edges of the sample are found and correlated to determine sample length. The left (a) panel shows an example radiograph with a selected region illustrated by the red box. The right (b) panel shows this region from consecutive radiographs with pressure increasing to the left. Initial sample length is indicated by the horizontal lines. (Color online.)

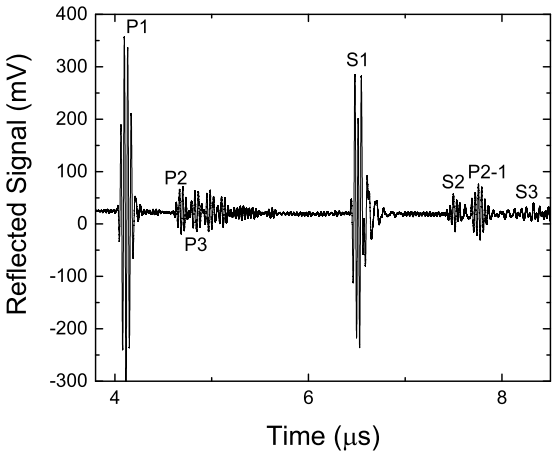

FIG. 4. Ultrasonic interferograms were generated from the interfaces between the solid, dense, polished materials between the sample and the exterior of the pressurized assembly. Labels above the individual reflections indicate the type of reflection it is (P is compressional and S is shear). To determine transit times, the pulses are overlapped with the previous pulse (i.e. P3 over P2 results in sample compressional transit time).

for the contrast shift midpoint between the sample and the surrounding material. Once the edges are mapped, the slopes are correlated between the top and bottom of the sample and a least-squares fit used to determine the sample length. This produces an error typically less than 1%. A pressure progression for the sample length is shown in Figure 3.

Ultrasonic interferograms were used to determine round trip transit times (t). Transit times are measured using the pulse-echo overlap technique[10–13] and have an associated error of half the smallest data time step, or 0.5 ns. Together, the sample lengths and transit times are used to determine sound velocities in the material.

Sound velocities are calculated as $\nu_x = \frac{2L}{t_x}$, with x des-

ignating either p or s for compressional or shear. X-ray results were used to determine cell parameters and volumes, along with densities (ρ). Elastic moduli are determined from the compressional (longitudinal) and shear sound velocities and density as $m = \rho\nu_m^2$, where m is used to represent L (longitudinal modulus) or G (shear modulus). Adiabatic bulk moduli are determined at each pressure point from the other two moduli as $B = L - 4/3G$.

Beyond just the elastic parameters, there are methods for determining several thermal parameters from the sound velocity and x-ray results. These include the elastic Debye temperature[18,19], Grüneisen parameter[20], acoustic thermal conductivity[21], and the isothermal bulk modulus[12]. In particular, the elastic Debye temperature, lattice thermal conductivity, and Grüneisen parameter are computed starting from the average/mean sound velocity, which is computed as

$$\nu_m = \left(\frac{\nu_p^{-3} + 2\nu_s^{-3}}{3} \right)^{-1/3}. \quad (1)$$

From this mean sound velocity, the elastic Debye Temperature is determined from

$$\Theta_{D,elastic} = \frac{h}{k_b} \left(\frac{3N_A\rho}{4\pi a} \right)^{1/3} \nu_m \quad (2)$$

with a being the atomic weight, h being the Planck constant, and ρ being the density. The Grüneisen parameter is determined directly from the sound velocities through

$$\gamma = \frac{3}{2} \left(\frac{3(\nu_l/\nu_s)^2 - 4}{(\nu_l/\nu_s)^2 + 2} \right). \quad (3)$$

The elastic Debye temperature is then used to compute the Acoustic Thermal Conductivity as

$$\lambda_{lat} = 8 \left(\frac{k_b}{h} \right)^3 \frac{MV^{1/3}\Theta_D^3}{\gamma^2 T} \quad (4)$$

with V being the unit cell volume, M the formula mass per unit cell, T being the temperature, and γ being the Gruneisen Parameter. Finally, the isothermal bulk modulus is determined as

$$K_{T0} = \frac{K_{S0}}{1 + \alpha\gamma T}. \quad (5)$$

In addition to the parameters reported in this paper, it is also possible to compute Young's modulus and the Poisson ratio from the acquired data, using standard formulae relating the Bulk and Shear moduli (or the Longitudinal moduli, if so desired).

III. RESULTS

X-ray results have been found to agree well with the reported ambient *Cmcm* structure[1,22]. Ambient cell parameters are listed in Table I, with the Birch-Murnaghan 3^{rd} order equation of state parameters, resulting from the equation of state fit. These fits were performed using the EOSFit GUI package[23]. From these, the x-ray determined density is found to be 18.99(1) $\frac{g}{cm^3}$. The equation of state and pressure-volume points are illustrated in Figure 5.

TABLE I. X-ray determined equation of state parameters for depleted uranium. These results were obtained by fitting a 3^{rd} order Birch-Murnaghan equation of state to the x-ray obtained volume-pressure data, using the EOSFit GUI program[23]. Errors are reported next to the digit the correspond to. Errors for the cell parameters are obtained from MDI JADE, where errors in the equation of state parameters are determined from EOSFit.

a (Å)	2.846(1)	V_0 (Å^3)	83.26(1)
b (Å)	5.898(1)	B_0 (GPa)	129(2)
c (Å)	4.958(1)	B_0'	5(1)

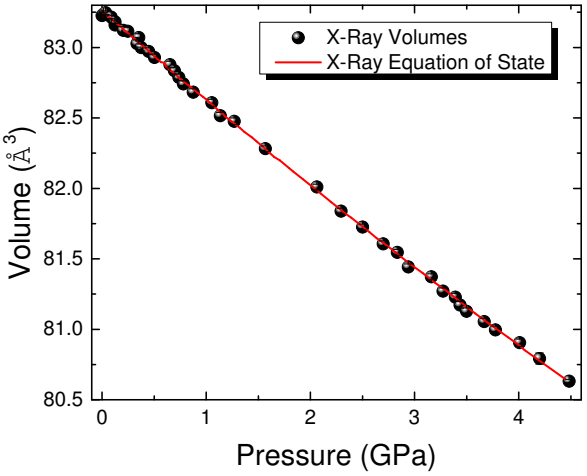

FIG. 5. The x-ray data collected was analyzed to determine a pressure-volume curve for depleted uranium metal. This plot also includes the Birch-Murnaghan equation of state fit to this data. Parameters for this fit are presented in Table I. Errors are represented by the size of the point in this figure. (Color online.)

Least squares fits to the ultrasonic results are listed in Table II, with plots of the sound velocities with pressure being previously reported[14]. These fits gives an ambient shear modulus of 74 GPa and a longitudinal modulus of 231 GPa. In each case, the parameter values and pressure derivatives are illustrated in Table II and indicate varying degrees of increase with applied load.

Calculation of the thermal parameters has also been performed from Eqns. 1 to 5. The results shown of this calculation are shown in Figure 7. As with the elastic results, ambient values are in Table II. Using volumetric thermal expansion[24], the isothermal bulk modulus is computed to be 131.1(1) GPa and increases slowly with applied pressure.

TABLE II. Ultrasonically determined elastic and thermal parameters for depleted uranium. Estimated errors in these parameters are shown in parentheses after the digit they represent error in. All errors are determined from linear least-squares fits to the pressure data obtained.

Property	Ambient Pressure Value	High Pressure Slope
ν_p (km/s)	3.488(1)	0.038(1)
ν_s (km/s)	1.979(1)	0.026(1)
L (GPa)	230.9(2)	7.07(8)
G (GPa)	74.5(1)	2.26(3)
B (Adiabatic, GPa)	131.9(1)	3.62(5)
θ_D (K)	327.7(2)	5.05(6)
γ	1.56(1)	-0.007(1)
$\lambda_{acoustic}$ (W/m-K)	0.46(1)	0.026(1)
B_0 (Isothermal, GPa)	131.1(1)	3.59(4)

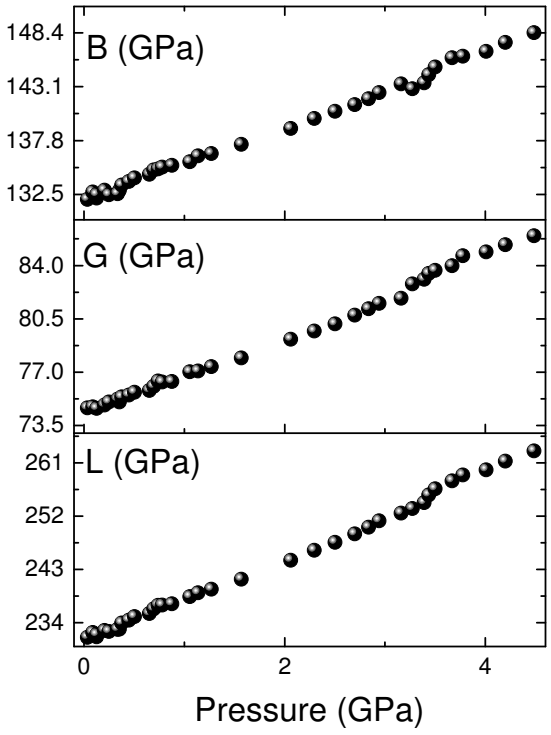

FIG. 6. Elastic moduli of U as a function of temperature. In this, the top panel is the Bulk Modulis (B_0), the middle is the Shear Modulus (G_0), and the bottom is the Longitudinal Modulus (L_0). Pressure is found to steadily increase the elastic moduli to the limit of experiment. While the data appears to show a localized change with applied load around 3.5 GPa, this is likely an artifact of the data and not a real feature of the results. Propagated errors in these parameters are represented by the size of the point.

IV. DISCUSSION

Previous measurements of bulk modulus for depleted uranium include static DAC measurements and shock studies[8,25–35]. However, these results are widely scattered, as is shown in Table III. In particular, it is seen

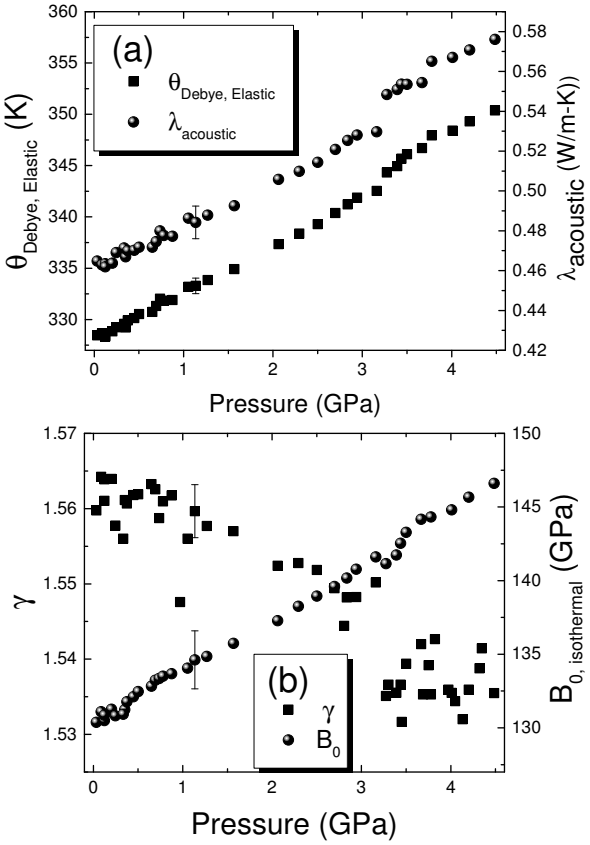

FIG. 7. Thermal parameters of uranium with pressure at ambient and elevated temperatures. The top (a) shows the determined elastic Debye temperature and acoustic component of the thermal conductivity. The bottom (b) shows the Grüneisen parameter, bottom and the isothermal bulk modulus. Representative errors are shown for each point.

from these results that the x-ray and ultrasound results form our work are consistent. It is not unusual to see variations in reported EOS parameters for uranium, or any other material in general, and this can be a result of a number of factors. For diamond anvil cell work, such as Akella[28] or Yoo[8], this variation is possibly associated with pressure medium effects. For example, pressure media are known to freeze with pressure increase. As a medium freezes, it begins to support shear waves and thus no longer provides a truly hydrostatic environment. Ultimately, as has been shown, non-hydrostatic stresses may lead to stiffer P-V behavior compared to the hydrostatic case. Such an explanation does not work in general for several reasons. As all pressure media will solidify at some pressure, there is no truly hydrostatic pressure medium. Additionally, such an argument is not applicable to the ultrasound work we present, as the pressure media are already solid. One principle effect of this is that is cannot be assumed to be purely hydrostatic. However, it is very likely to be quasi-hydrostatic and to remain so over the pressure range.

Therefore, it is more likely that such discrepancies are

TABLE III. Compilation of elastic and x-ray determined bulk moduli for depleted uranium. For this work, x-ray results were obtained by fitting a 3^{rd} order Birch-Murnaghan equation of state to the x-ray obtained volume-pressure data, using the EOSFit GUI program[23]. Errors are reported next to the digit the correspond to. Elastic bulk moduli are determined from the equations presented in the Experimental Details section using the Longitudinal and Shear moduli. Values in the upper portion of this table are experimental and the lower section shows theoretical results. All results (excluding those from this work) are ordered top to bottom from oldest to newest.

Reference	X-ray B_0 (GPa)	Elastic B_0 (GPa)
This Work	129 (2)	131.1(1)
Fisher *et al.*[25]		115
Merx *et al.*[26]	143	
Akella *et al.*[27]	125.0	
Akella *et al.*[28]	138.7	
Yoo *et al.*[8]	135.5	
Le Bihan *et al.*[30]	104	
Zhao *et al.*[31]	117-119	
Dewaele *et al.*[34]	115	
Soderlind[29]	130	
Taylor[32]	149	
Beeler *et al.*[33]	151	
Dewaele *et al.*[34]	129 (α)	
Dewaele *et al.*[34]	115 (α_1)	
Bouchet *et al.*[35]	129	

associated with the samples used. As such, it is difficult to comment on particular effects that could be responsible for the large range variations. One possibility is the lower moduli are associated not with the regular α phase, but with the α_1 phase. Evidence can be found for this in some of the reported results, such as the work of Dewaele[34], where their reported modulus mates well with their theoretical results for the α_1 phase. Grain size could, and probably does play a factor, as has been previously been argued by Lander *et al.*[36]. Other possibilities include a correlation between B_0 and B_0'[37] or the purity of the sample, known to have effects on the transition pressure and strength of zirconium[38]. Further work is planned to investigate these possibilities.

The elastic Debye temperature shows a steady increase with applied pressure, indicative of stiffening of the lattice and upward shifts of the phonon frequencies. The value found from these results (327.7 K) is slightly higher than theoretical determinations, which range from 228 to 300 K[4,29,33,39,40]. However, this difference likely only indicates slightly stiffer bonds than present in the calculations. Further comparison of results is presented in Table IV. In this table, we present both low-temperature limits[4,36,39] and ambient temperature values[29,32,33,40]. From these results, it is easily seen that the low-temperature results show a discrepancy between the elastically determined Debye temperature and that from heat capacity of at least 40 K. In contrast, the ambient temperature values deviate from our value (determined directly from sound velocities) by at minimum

TABLE IV. Comparison of low-temperature limit and ambient temperature determined Debye temperatures for depleted uranium. Calculation of the Debye temperature from sound velocities is performed using Eqn. 2. The upper portion of this table shows experimental results, the middle portion is compiled results in a review paper, and the bottom results are theoretical. All results (excluding those from this work) are ordered top to bottom from oldest to newest.

Reference	Low-T Limit (K)	Ambient (K)
This Work		327.7(2)
Fisher *et al.*[4]	251	
Fisher *et al.*[39]	248	
Ho *et al.*[40]		300
Lander *et al.*[36]	182.6-218	
Soderlind[29]		228
Taylor[32]		287
Beeler *et al.*[33]		287

27 K. Again, as previously discussed, it is possible and likely that the difference at the low-temperature limit remains at ambient temperature.

Similar behavior is observed for the acoustic thermal conductivity, which amounts to nearly 0.5 $\frac{W}{m-K}$ under ambient conditions. Previously, the total thermal conductivity was reported[41] to range from 20 to 30 $\frac{W}{m-K}$. It is well known that the thermal conductivity in most materials can be considered dominated by acoustic phonon and electronic conduction[42]. However, other contributions can present the dominant portion of the thermal conduction in a material. For uranium, the electrical resistivity can be used to obtain an estimate of the electronic contribution to the thermal conductivity through the Wiedemann-Franz equation. Assuming a theoretical Lorenz number (i.e. $L_0 = 2.44\ \mu\Omega$-mΩ/K^2), the reported resistivity of approximately 25 $\mu\Omega$-cm[43] translates into a thermal conductivity of 29.28 $\frac{W}{m-K}$, which is very close to the reported values.

Changes in bonding with pressure are also evident in the Grüneisen parameter. In this case, the decreasing trend with applied load suggests a decreasing anharmonic component. It is known that increasing temperature results in an increase of the anharmonicity exhibited by uranium metal[44,45]. However, pressure is generally expected have the opposite effect (i.e. lowering temperature is similar to increasing pressure), in agreement with our observations. Our search of the available literature on the topic has not yielded any previous reports of this parameter for the α structure at ambient temperature. Such a result directly implies that pressure is more strongly localizing the atomic oscillations to the crystallographic site, but further exploration of this phenomenon is required to give better detail.

V. CONCLUSIONS

We have performed the first high pressure ultrasonic study of depleted uranium metal with pressure. This study has covered the pressure range up to 4.6 GPa and has resulted in combined x-ray radiographic and diffractive and ultrasonic interferometric measurements of the sample. From this, an x-ray pressure-volume curve and sound velocities have been determined.

These sound velocities and x-ray densities have been used to obtain elastic moduli. Further, various thermal parameters and conversion between the adiabatic and isothermal bulk modulus have resulted from these elastic moduli and external data[24]. It has been found that pressure generally has the impact of increasing material strength and elastic moduli. The sole exception to this is the decrease in the Grüneisen parameter with applied load. Overall, the parameters determined are found in good agreement with previous reports, where these are available.

In addition to the first set of elastic/thermal results on uranium metal at high pressure, this work has also demonstrated the capacity to make such measurements on radioactive and other potentially hazardous materials. This first application of a previously reported containment setup allows the study of radioactive materials through these techniques[14]. While groundbreaking in the study of radioactive metals and compounds, future study is required to further determine the pressure-temperature evolution of such materials.

ACKNOWLEDGMENTS

Los Alamos National Laboratory (LANL) is operated by LANS, LLC for the DOE-NNSA under contract no. DE-AC52-06NA25396. The authors acknowledge funding support from LANL Science Campaigns 1 and 2. Portions of this work were performed at HPCAT (Sector 16), Advanced Photon Source (APS), Argonne National Laboratory. HPCAT operations are supported by DOE-NNSA under Award No. DE-NA0001974 and DOE-BES under Award No. DE-FG02-99ER45775, with partial instrumentation funding by NSF. APS is supported by DOE-BES, under Contract No. DE-AC02-06CH11357. Use of the Advanced Photon Source, an Office of Science User Facility operated for the US Department of Energy (DOE) Office of Science by Argonne National Laboratory, was supported by the US DOE under Contract No. DE-AC02-06CH11357. MKJ gratefully acknowledges the support of the U.S. Department of Energy through the LANL/LDRD Program and the G.T. Seaborg Institute for this work. The authors also thank Dr. Baosheng Li for the use of his pulse-echo overlap software for determination of transit times.

[1] H. L. Yakel, in *Physical Metallurgy of Uranium Alloys* (Vail, Colorado, USA, 1974).
[2] J. Akella, S. Weir, J. M. Wills, and P. Söderlind, Journal of Physics: Condensed Matter **9**, L549 (1999).
[3] J. O. Snihs and G. Åkerblom, *Use of Depleted Uranium in Military Conflicts and Possible Impact on Health and Environment*, Tech. Rep. (1999).
[4] E. S. Fisher and H. J. McSkimin, Physical Review **124**, 67 (1961).
[5] J. C. Ho, N. E. Phillips, and T. F. Smith, Physical Review Letters **17**, 694 (1966).
[6] K. Andres, Physical Review **170**, 614 (1968).
[7] S. Raymond, J. Bouchet, G. H. Lander, M. Le Tacon, G. Garbarino, M. Hoesch, J.-P. Rueff, M. Krisch, J. C. Lashley, R. K. Schulze, and R. C. Albers, Physical Review Letters **107**, 136401 (2011).
[8] C.-S. Yoo, H. Cynn, and P. Söderlind, Physical Review B **57**, 10359 (1998).
[9] C. J. Wu and P. Söderlind, MRS Proceedings **1683** (2014), 10.1557/opl.2014.528.
[10] H. J. McSkimin, The Journal of the acoustical society of America **33**, 12 (1961).
[11] B. Li, J. Kung, and R. C. Liebermann, Physics of the Earth and Planetary Interiors **143**, 559 (2004).
[12] Y. Kono, A. Yamada, Y. Wang, T. Yu, and T. Inoue, Review of Scientific Instruments **82**, 2 (2011).
[13] Y. Kono, C. Park, T. Sakamaki, C. Kenny-Benson, G. Shen, and Y. Wang, Review of Scientific Instruments **83**, 033905 (2012).
[14] M. K. Jacobsen and N. Velisavljevic, Review of Scientific Instruments **86**, 113904 (2015).
[15] S. Speziale, C.-S. Zha, T. S. Duffy, R. J. Hemley, and H.-K. Mao, Journal of Geophysical Research **106**, 515 (2001).
[16] I. Materials Data, "Jade," (2015).
[17] WaveMetrics, "Igor Pro," (2015).
[18] G. Love, C. Koch, H. Whaley, and Z. McNutt, Journal of the Less Common Metals **20**, 73 (1970).
[19] H. Ledbetter, M. Lei, and S. Kim, Phase Transitions **23**, 61 (1990).
[20] D. S. Sanditov, M. V. Darmaev, B. D. Sanditov, and V. V. Mantatov, Russian Physics Journal **52**, 386 (2009).
[21] M. K. Jacobsen, W. Liu, and B. Li, Review of Scientific Instruments **83**, 093903 (2012).
[22] E. F. Sturcken and B. Post, Acta Crystallographica **13**, 852 (1960).
[23] R. J. Angel, "EOSFit," (2015).
[24] T. Lloyd, Journal of Nuclear Materials **3**, 67 (1961).
[25] E. S. Fisher, Journal of Nuclear Materials **18**, 39 (1966).
[26] H. Merx and C. Moussin, *High Pressure Science and Technology*, edited by B. Vodar and P. Marteau (Pergamon Press, 1979) p. 204.
[27] J. Akella, G. Smith, and H. Weed, Journal of Physics and Chemistry of Solids **46**, 399 (1985).
[28] J. Akella, G. S. Smith, R. Grover, Y. Wu, and S. Martin, High Pressure Research **2**, 295 (1990).
[29] P. Söderlind, Physical Review B **66**, 085113 (2002).
[30] T. Le Bihan, S. Heathman, M. Idiri, G. Lander, J. Wills, A. Lawson, and A. Lindbaum, Physical Review B **67**, 134102 (2003).
[31] Y. Zhao, J. Zhang, D. Brown, D. Korzekwa, R. Hixson, and L. Wang, Physical Review B **75**, 174104 (2007).
[32] C. Taylor, Physical Review B **77**, 094119 (2008).
[33] B. Beeler, C. Deo, M. Baskes, and M. Okuniewski, Journal of Nuclear Materials **433**, 143 (2013).
[34] a. Dewaele, J. Bouchet, F. Occelli, M. Hanfland, and G. Garbarino, Physical Review B **88**, 134202 (2013).
[35] J. Bouchet and F. Bottin, Physical Review B **92**, 174108 (2015).
[36] G. Lander, E. Fisher, and S. Bader, Advances in Physics **43**, 1 (1994).
[37] S. Adak, H. Nakotte, P. de Châtel, and B. Kiefer, Physica B **406**, 3342 (2011).
[38] N. Velisavljevic, G. N. Chesnut, L. L. Stevens, and D. M. Dattelbaum, Journal of Physics: Condensed Matter **23**, 125402 (2011).
[39] E. S. Fisher and D. Dever, Physical Review **170**, 607 (1968).
[40] C. Y. Ho, R. W. Powell, and P. E. Liley, Journal of Physical and

Chemical Reference Data **3** (1974).
[41] T. A. Sandenaw, *Thermal Conductivity of Uranium: Effects of Purity and Microstructure*, Tech. Rep. LA-6092-MS (Los Alamos National Laboratory, Los Alamos, NM, 1975).
[42] J. M. Ziman, *Electrons and phonons: the theory of transport phenomena in solids*, edited by N. F. Mott, R. C. Bullard, and D. H. Wilkinson, Vol. 20 (Oxford at the Clarendon Press, 1960) p. 555.
[43] S. Arajs, R. H. Flora, and E. E. Anderson, Journal of Nuclear Materials **37**, 89 (1970).
[44] M. E. Manley, Los Alamos Science , 202 (2000).
[45] M. E. Manley, B. Fultz, R. J. McQueeney, C. M. Brown, W. L. Hults, J. L. Smith, D. J. Thoma, R. Osborn, and J. L. Robertson, Physical Review Letters **86**, 3076 (2001).